Setting Adaptive Inspection Intervals in Helicopter Components, Based on a Digital-Twin

Fubin Zhao,[*] Xuan Zhou,[†] Chaoyang Wang,[‡] and Leiting Dong[§]
Beihang University, 100191 Beijing, People's Republic of China

and
Satya N. Atluri[**]
Texas Tech University, Lubbock, Texas 79409

Setting inspection intervals based on an accurate prediction of fatigue crack sizes is essential for sustaining the integrity of aeronautical structures. However, the fatigue crack growth and its prognosis are affected by various uncertainties, which makes the current inspection strategy with fixed intervals challenging in managing the aircraft with diverse damage states in a fleet. In this study, an intelligent crack inspection strategy is proposed based on a digital twin, in which a reduced-order fracture mechanics simulation methodology, a validated fatigue crack growth model, and the historical crack length inspection results are integrated into a dynamic Bayesian network. The proposed strategy utilizes two connected probabilistic processes, which conduct the diagnosis/prognosis and calculate the inspection intervals, respectively, to adaptively set the inspection intervals according to the updating of the digital twin model. The proposed inspection strategy is demonstrated by the various crack growth histories of a helicopter component and benchmarked against several baselines. The results show that the probability of failure (PoF) can be kept below the threshold, even though the initial crack size and the crack growth parameters are underestimated in the prior

[*] Ph.D. candidate, School of Aeronautic Science and Engineering.
[†] Ph.D. candidate, School of Aeronautic Science and Engineering, also Ph.D. candidate at the Department of Mechanical Engineering, Politecnico di Milano, Milano, 20156, Italy; zhoux@buaa.edu.cn (Corresponding author).
[‡] Ph.D. candidate, School of Aeronautic Science and Engineering.
[§] Professor & Deputy Dean, School of Aeronautic Science and Engineering; ltdong@buaa.edu.cn (Corresponding author).
[**] Presidential Chair & University Distinguished Professor, Mechanical Engineering. Fellow AIAA.

distribution. Further applications on more realistic aircraft structures will be carried out in the future.

Nomenclature

t = time step

$\boldsymbol{X}_t$ = state variables at time step t

$\boldsymbol{v}_t$ = vector of noise terms in the state function at time step t

$\boldsymbol{Z}_t$ = measurement variables at time step t

$\boldsymbol{n}_t$ = vector of noise terms in the observation function at time step t

$\boldsymbol{a}_t^0$ = crack lengths before time step t

$\Delta\boldsymbol{a}$ = increment of crack lengths at time step t

$\boldsymbol{a}_t$ = crack lengths after time step t

$\Delta\boldsymbol{K}$ = ranges of stress intensity factors

K_c = fracture toughness

$\boldsymbol{\mu}$ = material parameters related to the crack growth

σ_{base} = reference load

a_t^{surf} = length of surface crack at time step t

a_{obs_t} = observation of crack length at time step t

ε_t = random variables in the measurement equation of traditional methods at time step t

ω_t = noise term in random crack growth process at time step t

σ_ω = standard deviation of distribution of ω_t

ΔN = cycle increment between adjacent time steps

$\boldsymbol{\sigma}_\varepsilon$ = standard deviations of measurement results

C, γ = material parameters in generalized Frost-Dugdale law

ΔP = fatigue load

a_d = detectable threshold of crack size

a_e = economic repair crack size

a_c = critical crack size

N_{det} = number of detections during an inspection

N_{hit} = hit number in detections during an inspection

z_t^{pod} = observation of probability of detection at time step t

ε_t^{PoD} = measurement noise of the NDI equipment at time step t

N_s = number of particles in regularized particle filter algorithm

I. Introduction

MOST of the structural failures in aircraft are due to fatigue fracture, in which cyclic fatigue loads cause cracks to initiate in a fatigue critical component and grow eventually, affecting the structural integrity. Prognosis of the fatigue crack growth and remaining useful life (RUL) is desired to devise inspection strategies that can reduce unexpected downtime as well as unnecessary scheduled maintenance [1, 2]. The traditional aircraft structural inspection strategy is based on the safety management philosophy of damage tolerance, by which the fixed inspection interval is devised according to the design load spectrum, crack growth analysis, and test results [3]. However, this strategy does not consider the influence of various uncertainties on fatigue crack growth. On the one hand, from the perspective of damage evolution in physical structures, each aircraft undergoes a different load history, which is caused by its mission diversity and pilot habits, and each aircraft's geometric and material properties vary to a certain degree during manufacturing, both of which lead to a different trajectory of damage evolution for each aircraft than for other aircraft in the fleet [4]. On the other hand, from the point of view of structural damage prognosis, it is difficult to acquire the true values of geometric and material properties. Although the nominal values used to calculate the damage evolution can be obtained from the manufacturer [5], these are still slightly different. In order to effectively track the damage evolution and formulate a more reasonable inspection strategy, it is necessary to comprehensively consider the influence of various uncertainties on the damage evolution.

The individual aircraft tracking (IAT) program has been widely implemented on many types of aircraft in recent years [6-8]. With the recorded flight data from the installed data acquisition unit [9], it aims to track the potential

fatigue damage growth and life consumption for each aircraft in a fleet. However, most IAT systems in engineering practice only monitor load data such as aircraft overload, while epistemic uncertainties that also lead to discrepancies in damage states, such as geometric and material parameters, are not considered. The U.S. Air Force has been funding research on the airframe digital twin (ADT), which is an extension of the IAT, also known as Probabilistic and Prognostic Individual Aircraft Tracking (P^2IAT) in Spiral 1 of the project. ADT enables structural damage diagnosis and prognosis by creating a multiphysics, multiscale, and probabilistic virtual model [10] of an as-built system that can integrate multiple heterogeneous and uncertain sources of information from models and data to support decisions for proactive fleet maintenance [4, 11-13]. In 2009, the National Research Council of Canada proposed a roadmap for probabilistic life usage monitoring for helicopters [14], which can be regarded as a preliminary concept of the helicopter digital twin. Millwater [13] systematically described the probabilistic methods required for the application of digital twins to aircraft structures, the current research status, and future challenges.

In the realization of the digital twin for aeronautical structures, it is a critical step to diagnose the current damage state of the system and prognose the future damage evolution. The Dynamic Bayesian Network (DBN) has been widely adopted as the framework of diagnosis and prognosis in current digital twin studies of various objects, such as the aircraft wing [4], orthotropic steel deck [15], and reusable spacecraft structures [16]. Yu [17] established a digital twin model based on non-parametric Bayesian networks to describe the dynamic degradation process of structural health states in which the Gaussian particle filter (GPF) and Dirichlet process mixture model (DPMM) are adopted to enhance the model adaptability. In [18-20] the DBN framework is utilized to develop an component health-and stress-aware system control strategy based on digital twin, in which the load profile or the flight parameter is optimized under uncertainties to satisfy the damage tolerance requirement in a certain maintenance-free operation period. However, most DBN applications are limited to the cases with simple crack shapes.

In this study, an adaptive crack inspection strategy based on a digital twin is proposed, which includes two probability processes with shared distributions of crack growth parameters. The primary process is used to diagnose and prognose the damage state of the component, and the secondary process, inherited from the probabilistic damage tolerance, is used to determine the inspection interval. A typical helicopter lifting frame is used to illustrate the method and framework. The results show that the PoF can be kept below the threshold, even though the initial crack size and the crack growth parameters were underestimated in the prior distribution. The main contributions of this work are summarized as follows:

1) Benefiting from the advantages of a previously developed real-time reduced-order modeling (ROM) method for complex structures [21], a DBN-based digital twin model is constructed to handle the diagnosis and prognosis of the complex crack growth in complex structures, which is not reported in the previous literature. The DBN can account for multiple uncertainties, providing a powerful tool for the implementation of the inspection strategy.
2) A novel strategy to set adaptive inspection intervals based on the digital twin is proposed. In contrast to the conventional damage tolerance, the crack growth parameters in the second process can be updated according to the first process. It is worth mentioning that in this study, the inspection interval is adjusted dynamically, which is different from [18-20] in which the inspection interval is fixed while the load profiles, the flight parameter, or the operational controls are adjusted.
3) The proposed strategy is benchmarked against several baselines, including fixed inspections without update, fixed inspections with update, and the single-process EIFS-PoF-based inspection strategy [13] to fully demonstrate the effectiveness of the strategy.

The remainder of this paper is organized as follows. Section II introduces the framework of the adaptive inspection strategy based on the concept of the digital twin. In Section III, the details of the helicopter component used to demonstrate the proposed strategy are provided, and its ROM construction is briefly described. In Section IV, the experiment data of the helicopter component is used to validate the digital twin model. In Section V, the proposed adaptive inspection strategy is demonstrated with a group of hypothetical crack growth histories and benchmarked against other inspection strategies. Finally, this study is completed with some concluding remarks in Section VI.

II. The Framework of the Proposed Adaptive Inspection Strategy Based on the Reduced-Order Digital Twin of Complex Structures

In this section, the proposed adaptive inspection strategy is introduced in detail. Firstly, the basic framework and its flowchart are introduced. Then, in Section II.A, we briefly describe a previously developed reduced-order modeling approach for fracture mechanics simulation of complex structures to tackle the rapid computation of state equations in the DBN framework. The DBN framework integrating the ROM and considering the partial observation is established in Section II.B. In Section II.C, the intelligent inspection and maintenance decisions based on the digital twin model are provided.

The traditional inspection strategy adopts fixed inspection intervals which are obtained by utilizing the damage tolerance philosophy for repairing or replacing critical components of the fixed-wing structure before the residual strength decreases to the specified level [13, 25], which is also applied to helicopters [3, 26, 27]. Because the load history experienced by each aircraft within a certain interval is different and its own damage related properties vary, the fixed-interval inspection, which does not consider the influence of various uncertainties, may be arranged earlier or later as compared to the true damage state of each aircraft, leading to economic or safety issues, respectively. In order to alleviate this problem, a crack inspection strategy based on digital twins is proposed in this study, which can provide more reasonable adaptive inspection intervals according to a constantly updated digital twin model.

The framework of the proposed strategy is shown in the figure below, including the off-line construction stage and the on-line use stage. It is worth mentioning that the proposed strategy can be considered an extension of the current strategy based on the philosophy of damage tolerance, which can thus be easily adopted in the usage of in-service aircraft.

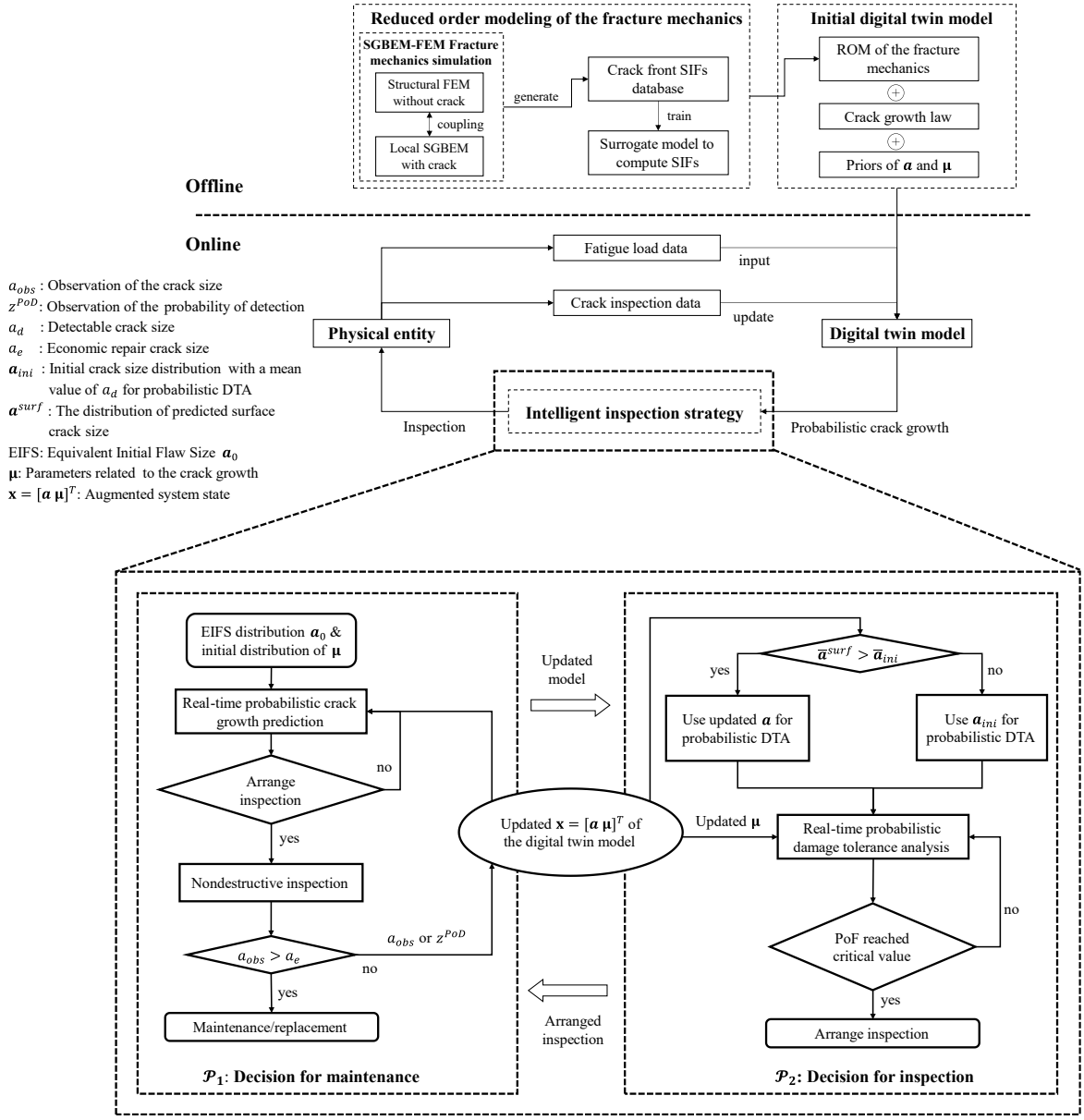

Fig. 1 The framework of the proposed intelligent inspection strategy.

In the off-line construction stage, the initial digital twin model is established based on the ROM. Firstly, a set of crack samples is generated by sampling along the possible crack growth path [27]. Subsequently, the symmetric Galerkin boundary element method - finite element method (SGBEM-FEM) coupling method [28-30] is used to calculate the stress intensity factors (SIFs) at the front nodes of all the crack samples to obtain the simulation database of fracture mechanics. The ROM of the fracture mechanics is constructed by the surrogate method. By combining the ROM and the crack growth model, real-time prediction of crack growth in complex structures can be achieved with the minimum computational cost. Based on practical experience, reasonable prior distributions for initial crack size

and crack growth model parameters are set to account for the various uncertainties. The ROM of the fracture mechanics and the crack growth model, together with the prior distribution of uncertain parameters, constitute the initial digital twin model.

In the stage of online use, the fatigue load data is acquired as the input for the digital twin model. Two probabilistic crack growth processes are carried out simultaneously, which receive the same statistical fatigue load and share the same distribution of damage-related parameters. The primary process $\mathcal{P}_1$ is used to conduct the diagnosis and prognosis of the individual component, in which the initial crack distribution starts from the EIFS and uncertain damage related parameters are considered. The secondary process $\mathcal{P}_2$ is adopted to perform the probabilistic damage tolerance analysis (DTA) to determine the inspection intervals.

A. Reduced-Order Crack Growth Prediction in Complex Structure

To meet the timeliness requirements of probabilistic crack growth prediction, it is necessary to construct a ROM of fracture mechanics simulation to efficiently predict SIFs of all nodes on a crack front, which can be called upon repeatedly within the Bayesian probability frameworks. For this problem, the time of full-order simulation is between tens and hundreds of seconds, while it only takes a few milliseconds to call the ROM [21]. The construction process of ROM in this paper is described as follows. Interested readers can refer to [21] for more details:

1) Generate a set of samples by sampling on the possible crack growth path, and the crack size of each sample is different.

2) Apply the reference load σ_{base} to all samples and calculate the SIFs of all nodes on each crack front rapidly by the SGBEM-FEM coupling method.

3) Taking the crack sample parameters (i.e., coordinates of all nodes on the crack front) as the input and the corresponding SIFs as the output, train the ROM of fracture mechanics simulation by regression methods.

In order to accelerate the construction of the crack database, an efficient method, the SGBEM-FEM coupling method, which combines the advantages of the finite element method (FEM) and the boundary element method (BEM), is adopted. The FEM, which can efficiently simulate complex structures, is used to simulate the region without cracks in the complex structure, and the SGBEM super element, which can accurately calculate the SIFs and efficiently simulate the crack growth, is used to simulate the local subdomain with cracks. The two kinds of discretization are directly coupled through the stiffness matrix.

B. Dynamic Bayesian Network for Crack Growth Diagnosis and Prognosis

In order to comprehensively consider the effects of aleatory and epistemic uncertainties on crack growth, it is necessary to explore methods that can integrate various uncertainties. The DBN is an extension of the Bayesian network in the time domain, which is effective for integrating various sources of uncertainty and heterogeneous information and tracking the changes of state of time-variant systems. When the observation of any child node is acquired, the DBN is updated by Bayesian inference.

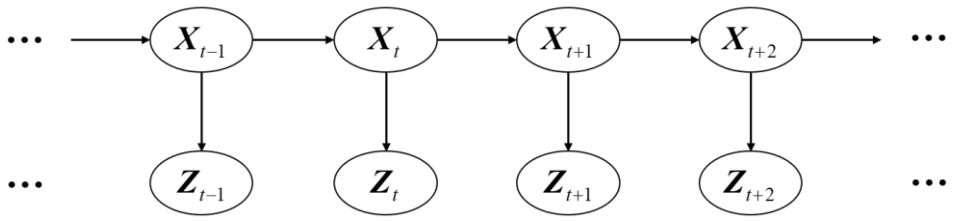

Fig. 2 A simple DBN, the state of current BN depends only on BN at the previous time step based on the first order Markov hypothesis.

Fig. 2 shows a simple DBN representation of a degradation process. The state variables at time step t are denoted as $\boldsymbol{X}_t \in \Re^m$, which evolve from state variables $\boldsymbol{X}_{t-1} \in \Re^m$ at time step t-1 according to the state function:

$$\boldsymbol{X}_t = f(\boldsymbol{X}_{t-1}, \boldsymbol{v}_{t-1}) \tag{1}$$

where $\boldsymbol{v}_{t-1} \in \Re^m$ denotes the vector of noise terms in the state function. The measurement at time step t is denoted as $\boldsymbol{Z}_t \in \Re^n$, which is obtained according to observation function:

$$\boldsymbol{Z}_t = h(\boldsymbol{X}_t, \boldsymbol{n}_t) \tag{2}$$

where $\boldsymbol{n}_t \in \Re^n$ denotes the vector of noise terms in the observation function.

In order to effectively track the evolution process of state variables $\boldsymbol{X}_t$ in Fig. 2, the following two tasks need to be accomplished by Bayesian inference: (1) forward propagation, i.e., obtaining the state variables $\boldsymbol{X}_t$ according to the state variables $\boldsymbol{X}_{t-1}$ at the previous time step and the conditional probability distribution (CPD) between the networks at two adjacent time steps; and (2) backward inference, i.e., updating the joint probability distribution of the state variables $\boldsymbol{X}_t$ when any child node is observed.

For the crack growth problem, the state of the system is denoted by crack length vector $\boldsymbol{a}$. The fatigue crack growth law is as follows:

$$\frac{d\boldsymbol{a}}{dN} = f(\boldsymbol{a}, \Delta\mathbf{K}; \boldsymbol{\mu}) \tag{3}$$

where $\frac{d\boldsymbol{a}}{dN}$ are the increments of crack lengths per cycle, $\boldsymbol{a}$ are the crack lengths, $\Delta\mathbf{K}$ are the ranges of SIFs, $\boldsymbol{\mu}$ are the material parameters, which are considered as uncertain parameters in the DBN framework.

Appending unknown material parameters $\boldsymbol{\mu}$ to crack lengths $\boldsymbol{a}_t$ at time step *t*, the augmented state vector is defined as $\boldsymbol{X}_t = [\boldsymbol{a}_t \ \boldsymbol{\mu}_t]^T$. According to Eq. (3), the functional relationship of crack lengths between two adjacent time steps can be obtained as follows:

$$\boldsymbol{a}_t = \boldsymbol{a}_{t-1} + \frac{d\boldsymbol{a}_{t-1}}{dN}\Delta N \tag{4}$$

Then the state function can be obtained:

$$\begin{bmatrix} \boldsymbol{a}_t \\ \boldsymbol{\mu}_t \end{bmatrix} = \begin{bmatrix} \boldsymbol{a}_{t-1} + \frac{d\boldsymbol{a}_{t-1}}{dN}\Delta N \\ \boldsymbol{\mu}_{t-1} \end{bmatrix} \tag{5}$$

The measurement of the crack lengths $\boldsymbol{a}_t$ is assumed as $\boldsymbol{Z}_t \sim N(\boldsymbol{a}_t, \boldsymbol{\sigma}_\varepsilon^2)$ to consider the measurement noise. However, due to the limitations of measurement tools, the full shape of the crack front cannot be accurately obtained. Sometimes only the crack length at the surface of the structure is available. Then the corresponding observation function is obtained:

$$z_t = a_t^{surf} + \varepsilon_t \tag{6}$$

where a_t^{surf} is the crack length at the node where the crack front intersects the structural surface, and random variable $\varepsilon_t \sim N(0, \sigma_\varepsilon^2)$. σ_ε is the standard deviation of measurement results, which is determined by the accuracy of measurement tools.

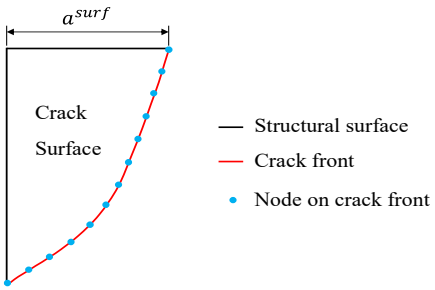

Fig. 3 A part-through crack surface, only the crack length on the upper surface can be observed.

This paper adopts the definitions of diagnosis step and prognosis step in [4], i.e., a time step with only forward propagation is defined as a "prognosis step"; and a time step with both forward propagation and backward inference is defined as a "diagnosis step". The diagnosis step is performed only when the inspection is conducted, and the prognosis step is performed in other cases. At the diagnosis step, the Bayesian inference algorithm is used to update the joint probability distribution of $\boldsymbol{X}_t$ based on the observation result.

Existing Bayesian inference algorithms include Kalman filtering [31], extended Kalman filter [31, 32], unscented Kalman filter [33-35], and particle filter [36, 37]. Different from the class of Kalman filters, the particle filter is widely used as the inference algorithm for DBN because of its ability to deal with non-Gaussian state variables [4, 15]. There are two challenges in the PF: 1) degeneracy, meaning that all but one particle will have negligible weights after a few iterations; and 2) sample impoverishment, meaning the loss of sample diversity. Methods to overcome these challenges include the regularized particle filter (RPF) and the kernel smoothing-based approach [36, 38]. In this paper, RPF is used as the Bayesian inference algorithm for DBN. For the complex structure considered in this paper, since only the length of the surface crack can be observed, $\boldsymbol{Z}_t$ reduces to z_t defined in Eq. (6), and the corresponding $\boldsymbol{a}_t$ in Eq. (5) is the coordinates of all nodes at the crack front. In other words, the position of the whole crack front as well as model parameters need to be updated with z_t.

C. Intelligent Inspection and Maintenance Decision Based on Digital Twin

To avoid the risk from inaccurate EIFS and accidental damage in the structural usage, an initial crack distribution $\boldsymbol{a}_{ini}$ (such as Weibull distribution) with a mean value of 1.27 mm, as defined in the probabilistic DTA [39, 40] and also known as the detectable threshold a_d, is adopted in $\mathcal{P}_2$ when the mean value of updated surface crack size $\bar{\boldsymbol{a}}^{surf}$ is smaller than a_d, which can prevent risks from occurring as a result of the true initial crack size and crack

growth parameters exceeding the assumed priori distribution or from accidental damage to the structure in service. Meanwhile, when $\bar{\boldsymbol{a}}^{surf}$ is larger than a_d, the crack size is considered to be measurable by Non-Destructive Inspections (NDI), and then the digital twin model in $\mathcal{P}_1$ can be updated with the observation. It is noted that the posterior crack distribution after the last observation is used for the initial crack distribution in $\mathcal{P}_2$ in this case. The inspection interval is then obtained when the PoF reaches a certain level.

However, because the length of the initial crack is usually about tens of microns [41], the crack size will be too small to measure in a traditional way for a long time during the usage, making it impossible to update the digital twin model in time. To address this issue, the observation of probability of detection (PoD) is adopted in this study to update the model when $\bar{\boldsymbol{a}}^{surf}$ is less than a_d.

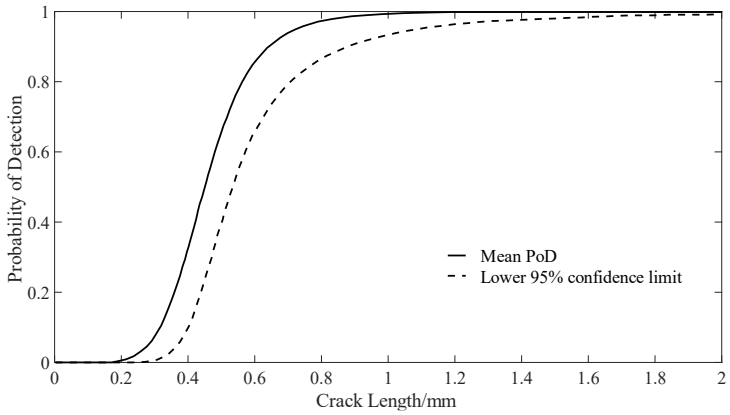

Fig. 4 A typical PoD curve and its lower 95% confidence limit, from [42].

Fig. 4 shows a typical PoD curve in which the PoD value increases strictly monotonically with crack length. When the crack size is smaller than a_d, the measurement of the crack size cannot be obtained by traditional methods, but the existence of a crack can be judged by the NDI equipment [43]. If the crack is detected, it is recorded as a hit; otherwise, it is recorded as a miss. If a number of N_{det} detections are performed during an inspection, and the total hit number is denoted as N_{hit}, then the observation of PoD is $\frac{N_{hit}}{N_{det}}$. Therefore, in the RPF algorithm, the observation function is replaced by:

$$z_t^{PoD} = PoD(a_t) + \varepsilon_t^{PoD} \tag{7}$$

where z_t^{PoD} denotes the observation of PoD, $PoD(\cdot)$ is the PoD function of the NDI equipment, ε_t^{PoD} is the measurement noise of the NDI equipment. The crack length of each particle is substituted into the PoD function to obtain the prediction of the PoD corresponding to the particle. Each particle is then weighted according to z_t^{PoD}, and the model is updated through the subsequent resampling process.

The updated damage related parameters are then shared with the secondary process $\mathcal{P}_2$ for the calculation of the next inspection interval. The above process is then repeated until the measured crack length exceeds the economic repair crack size a_e.

III. The Round-Robin Helicopter Lifting Frame and Its ROM for SIFs Prediction

In this study, a round-robin helicopter lifting frame [44] is adopted to illustrate the proposed intelligent inspection strategy. Its geometry, material, and subjected load spectra are introduced in Sections III.A to III.C, respectively. In Section III.D, the ROM for SIFs predictions is constructed [21].

A. Geometry Model

The geometry of the lifting frame is a flanged plate with a central lightning hole, with detailed dimensions shown in Fig. 5. There is a quarter-circular corner crack with a 2 mm radius located at the inner edge of the large central hole. The crack length a here is defined as the crack length on the upper surface of the lifting frame. The experimental results only show the evolution of the crack length a along the upper surface, but not the evolution of the full crack front.

B. Material and the Fatigue Crack Growth Law

The component is made of Al 7010-T73651, an aluminum alloy with a yield strength of 440 MPa, an average room temperature tensile strength of 502 MPa, and an average room temperature fracture toughness of 33.4 MPa$\sqrt{\text{m}}$ in the (L-T) orientation. In this paper, the component is assumed to have a Young's modulus of 70,000 MPa and a Poisson's ratio of 0.3 as in [27].

In this paper, a generalized version of the Frost-Dugdale law, which can calculate crack growth on the micron scale [45, 46], is used to describe crack growth in complex aircraft structures:

$$\frac{d\boldsymbol{a}}{dN} = C\boldsymbol{a}^{1-\gamma/2}\Delta\boldsymbol{K}^{\gamma} \tag{8}$$

where $\boldsymbol{a} = [a_1, a_2, \cdots, a_n]$ denotes the set of crack sizes at all nodes on the crack front, $\frac{d\boldsymbol{a}}{dN}$ denotes the increments in the crack lengths per cycle, C and γ are material parameters, and $\Delta\boldsymbol{K} = [\Delta K_1, \Delta K_2, \cdots, \Delta K_n]$ denotes the set of the ranges in the SIFs at all nodes on the crack front for that cycle. Vector $\boldsymbol{a}$ is used here because the crack front in a complex structure is an irregular curve, which needs to be characterized by multiple nodes. Therefore, the crack lengths at multiple nodes need to be considered within a crack surface. In [27, 46, 47], it was assumed that as a first approximation $\gamma = 3$, further in [27] $C = 1.28\times10^{-11}$ is inferred from the crack growth from 2 to 4 mm. In this study, material parameters C and γ are considered as uncertain parameters that need to be estimated.

C. Helicopter Load Spectra

In this paper, the Asterix spectra [27] are adopted. The average *R* value (stress ratio) of this stress spectrum is as high as 0.82. The largest far field stress in the spectrum was set to 130 MPa, which is consistent with the experiment [44]. The Asterix spectrum represents a single load block and corresponds to 190.5 flight hours (140 sorties).

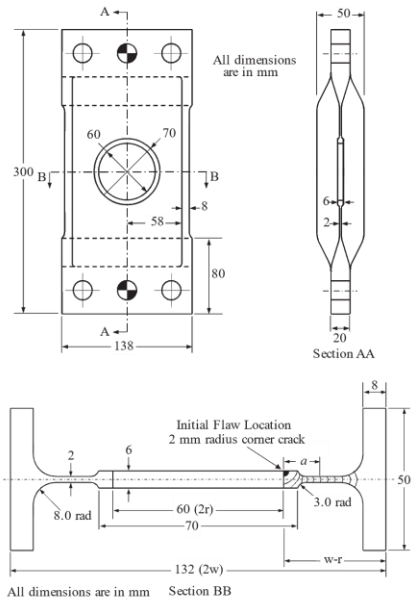

a) Schematic diagram of the helicopter lifting frame

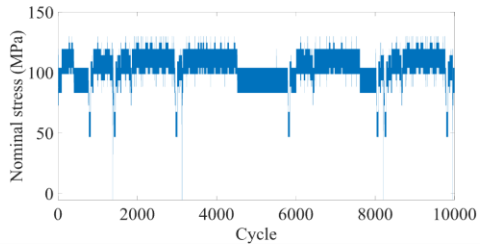

b) The Asterix load spectra

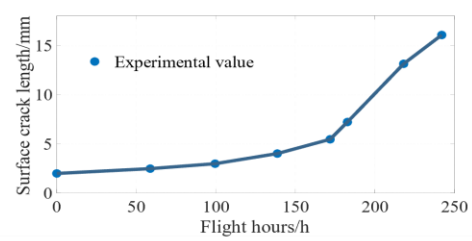

c) The test data of crack growth

Fig. 5 Geometry, load spectra and test data in the crack growth test, from [27, 48]. Adapted with permission from [21]. Copyright 2022 American Institute of Aeronautics and Astronautics. Adapted with permission from [48]. Copyright 2006 John Wiley and Sons.

D. Reduced-Order Model of the Fracture Mechanics Simulation

The construction of the ROM for the fracture mechanics simulation of the component is shown in Fig. 6. Interested readers can refer to [21] for more details.

In the offline construction of the database, the finite element model of the uncracked helicopter lifting frame, and the crack surface models with different shapes and sizes are established, which are combined as the inputs of the SGBEM-FEM coupling algorithm to automatically calculate the SIFs at the crack front. According to the geometric shape of the components, the whole crack growth process was divided into seven stages, and a certain number of crack samples were sampled at each stage. The nodal spacing equalization in [49] is conducted to obtain a consistent parametric characterization of different crack samples, allowing the relationship between the obtained SIFs and corresponding crack shapes/sizes to be established.

In the construction of the ROM, the dimension of crack front coordinates is projected to a low-rank subspace by the principal component analysis (PCA) to reduce the dimension of inputs, and the surrogate model is developed by regression methods. In this study, the artificial neural network (ANN) [50] is adopted. The error is defined as

$$\varepsilon = \frac{1}{q \times N} \sum_{i=1}^{q} \sum_{j=1}^{N} \frac{\left| y_{ij} - \hat{y}_{ij} \right|}{y_{ij}} \tag{9}$$

where N is the number of samples in training or test set, q is the number of nodes on a crack front, y is the SIFs obtained by the full-order simulation, $\hat{y}$ is the corresponding prediction by the ROM. The errors of all stages are summarized in Table 1. In practical, the effect of error can be considered by assuming $K \sim N(\hat{y}, (\hat{y} * \varepsilon)^2)$, where K is the SIF used to calculate the crack growth.

Table 1 The summary of errors

Stage	1	2	3	4	5	6	7
Number of samples N	881	288	239	67	347	87	760
Relative test error ε (%)	3.89	5.84	2.97	0.92	4.10	1.28	5.99

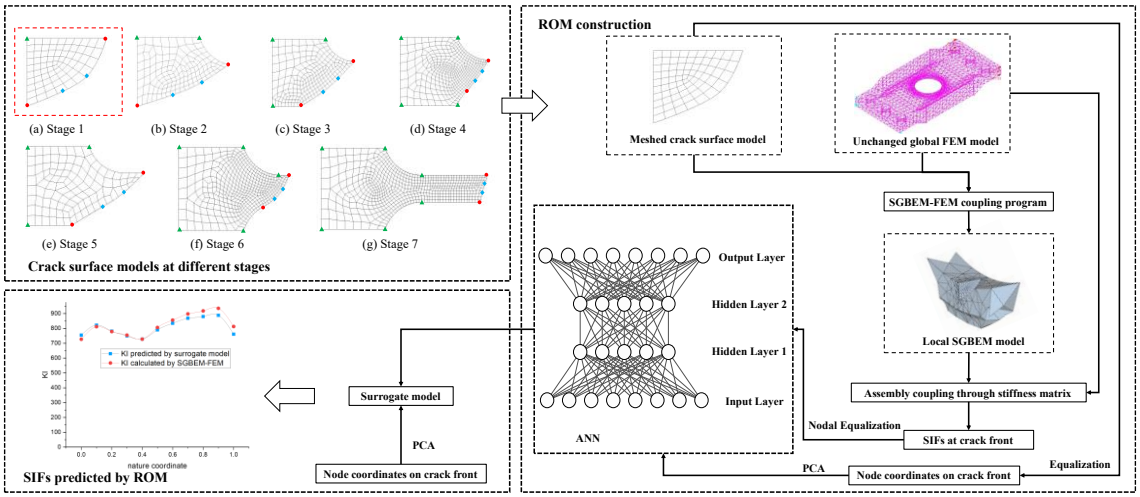

Fig. 6 ROM construction process for predicting stress intensity factors. Adapted with permission from [21]. Copyright 2022 American Institute of Aeronautics and Astronautics.

After obtaining SIFs, the increment and direction of the crack growth at each node are determined by the generalized Frost–Dugdale law and *J*-integral [51] respectively, which can be used to calculate the new crack front at the next time step.

IV. Probabilistic Diagnosis and Prognosis of the Component with Digital Twin

In this section, the diagnosis and prognosis of the crack growth in the helicopter lifting frame is conducted based on the digital twin and the experimental data from [27], which is a validation of the constructed digital twin model.

A. DBN for Crack Growth Analysis

In this study, the DBN for crack growth analysis is shown in Fig. 7. The subscript $t-1$ or t denotes the time step, and the corresponding symbols are explained in Table 2.

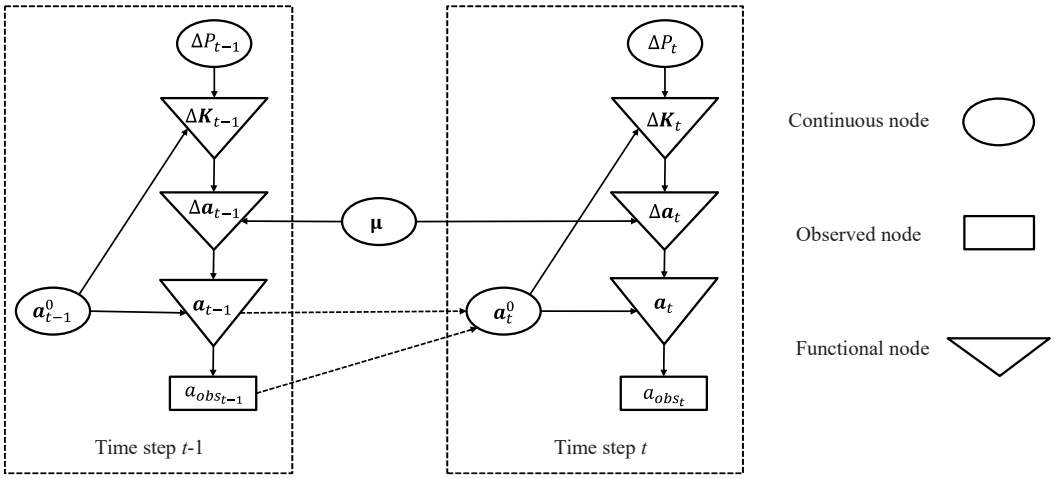

Fig. 7 DBN for crack growth analysis.

Table 2 The meaning of symbols in the DBN

Symbol	Meaning
ΔP	Range of the fatigue load
$\Delta \boldsymbol{K}$	Range of the stress intensity factors
$\Delta \boldsymbol{a}$	Crack increments at current time step
$\boldsymbol{a}^0$	Crack lengths before current time step
$\boldsymbol{a}$	Crack lengths after current time step
a_{obs}	Crack length observation
$\boldsymbol{\mu}$	Material parameters

In Fig. 7, an elliptical node represents a stochastic continuous node. A triangular node is a functional node, which means that given the value of parent nodes, the corresponding results can be obtained through a deterministic function calculation. A rectangular node represents an observed variable (e.g., the crack length). Solid arrows represent the functional relationships between variables within a BN slice, while dashed arrows represent functional relationships between variables across different time steps.

At time step 1, the distribution of random variables in the BN is the prior distribution provided by the user. The prior distribution of BN at other time steps is obtained by propagating the posterior distribution of BN at the previous time step. However, the prior distribution of $\boldsymbol{a}_t^0$ is determined by the following method:

1) If no crack length is observed at time step t-1, the prior distribution of $\boldsymbol{a}_t^0$ is equal to the predicted distribution of $\boldsymbol{a}_{t-1}$. Therefore, there is a dashed arrow pointing from $\boldsymbol{a}_{t-1}$ to $\boldsymbol{a}_t^0$ in Fig. 7.

2) If the crack length is observed at time step *t*-1, the prior distribution of $\boldsymbol{a}_t^0$ is updated based on the observation. Therefore, there is also a dashed arrow pointing from $a_{obs_{t-1}}$ to $\boldsymbol{a}_t^0$ in Fig. 7.

B. Digital Twin Initialization and Relevant Parameter Setting

In the adopted generalized Frost-Dugdale law, two parameters, i.e., C and γ, affect the accuracy of diagnosis and prognosis. In this paper, both C and γ are considered as uncertain parameters to be estimated. Due to the influence of measurement errors, the initial size of the crack in the component may not be exactly 2 mm but a certain deviation from it. In this paper, the initial size of the crack is also regarded as an uncertain parameter.

Based on the deterministic crack growth model Eq. (4), in order to consider the influence of process noise, the random crack growth process is described as [52, 53]:

$$\boldsymbol{a}_t = \boldsymbol{a}_{t-1} + \exp(\omega_{t-1}) \left.\frac{d\boldsymbol{a}}{dN}\right|_{t-1} \Delta N \tag{10}$$

where $\boldsymbol{a}_t$ are the crack lengths at time step *t*, ΔN is the number of load cycles experienced from time step *t*-1 to time step *t*, ω_{t-1} is a noise term following Gaussian distribution $N(-\frac{\sigma_\omega^2}{2}, \sigma_\omega^2)$, leading to $E(\exp(\omega_{t-1})) = 1$ [53, 54]. The crack growth rate $\left.\frac{d\boldsymbol{a}}{dN}\right|_{t-1}$ is expressed as follows:

$$\left.\frac{d\boldsymbol{a}}{dN}\right|_{t-1} = C_{t-1} \boldsymbol{a}_{t-1}^{1-\gamma_{t-1}/2} \Delta \boldsymbol{K}_{t-1}^{\gamma_{t-1}} \tag{11}$$

In Eq. (11), model parameters C and γ are replaced by C_{t-1} and γ_{t-1} respectively to consider the uncertainty of model parameters. According to the linear correlation between the coefficient and exponent in the power law equation of fatigue crack growth [55], the joint prior distribution of C and γ is set as $\left.\begin{bmatrix}\log(C_t)\\ \gamma_t\end{bmatrix}\right|_{t=0} \sim N\left(\begin{bmatrix}-10.9\\ 3\end{bmatrix}, \begin{bmatrix}0.15^2 & -0.05^2\\ -0.05^2 & 0.05^2\end{bmatrix}\right)$ due to insufficient knowledge. Here $\log(C_t)$ is used instead because C_t is a very small value compared to other quantities. The prior mean value of γ is set to 3 as defined in [27, 46, 47]. The prior distribution of the corner crack length is adopted as $a_t|_{t=0} \sim N(2, 0.1^2)$ to consider the

uncertainty of the initial crack size. The measurement error is set as $\varepsilon_t \sim N(0, 0.1^2)$ to consider the measurement uncertainty, and σ_ω^2 is set as 0.1 to consider the effect of process noise on the crack growth.

The number of particles is set as $N_s = 2000$ to balance the computational cost and simulation accuracy. At the initial time step $t = 0$, the particle set $\left\{\boldsymbol{x}_{t=0}^{(i)}\right\}_{i=1}^{N_s} = \left\{\boldsymbol{a}_{t=0}^{(i)}, \log C_{t=0}^{(i)}, \gamma_{t=0}^{(i)}\right\}_{i=1}^{N_s}$ is randomly sampled from the prior probability density functions (PDFs) mentioned above. After that, each particle $\boldsymbol{x}_t^{(i)} = [\boldsymbol{a}_t^{(i)}, \log C_t^{(i)}, \gamma_t^{(i)}]$ $(i = 1, 2, \cdots, N_s)$ evolves with time step. The increment of loading cycle in Eq. (10) is set as $\Delta N = 1000$ to balance the computational cost and the accuracy. When the time step corresponding to the experimental observation (i.e., the diagnosis step) is reached, the measurement of crack size from [27] is input into the DBN to obtain the posterior distribution for each parameter in state vector $\boldsymbol{X}_t = [\boldsymbol{a}_t, \log C_t, \gamma_t]$. The relevant parameters in this example are summarized in Table 3.

Table 3 Relevant Parameter Setting

Parameter	Value
Joint prior distributions of model parameters C and γ	$\left.\begin{bmatrix}\log(C_t)\\ \gamma_t\end{bmatrix}\right\|_{t=0} \sim N\left(\begin{bmatrix}-10.9\\ 3\end{bmatrix}, \begin{bmatrix}0.15^2 & -0.05^2\\ -0.05^2 & 0.05^2\end{bmatrix}\right)$
Prior distribution of the corner crack length	$a_t\big\|_{t=0} \sim N(2, 0.1^2)$
Measurement error	$\varepsilon_t \sim N(0, 0.1^2)$
Random noise term in crack propagation equation	$\omega_t \sim N(-\frac{\sigma_\omega^2}{2}, \sigma_\omega^2),\ \sigma_\omega^2 = 0.1$
Number of particles in the RPF algorithm	2000
Increment of loading cycle	$\Delta N = 1000$

C. Discussion of the Diagnosis and Prognosis Results

Fig. 8 shows the updates of the joint distribution of $\log C$ and γ with the inspections. Their joint distribution becomes narrower after several updates allowing a more accurate prediction of the crack growth process. The

distribution is not narrowed to a small range in both dimensions, indicating a strong correlation between the $\log C$ and γ. In the original set $\left\{\boldsymbol{x}_{t=0}^{(i)}\right\}_{i=1}^{N_s}$, the particles that do not conform to the real process are eliminated.

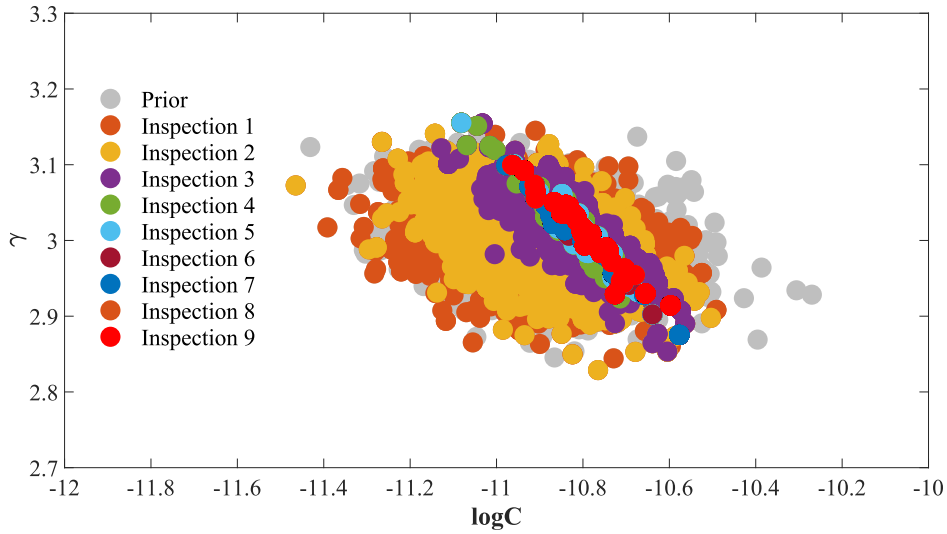

Fig. 8 Updating of joint distribution of logC and γ.

Fig. 9 shows the comparison of probabilistic crack growth with and without diagnoses. Compared with the case without diagnoses, the case with diagnoses can effectively reduce the uncertainty and track the actual growth process. The uncertainty of crack size distribution decreases at each inspection and increases gradually between two adjacent inspections. Table 4 shows the comparison between the crack growth prediction and the experimental observation at each diagnosis step. The results confirm that the proposed digital twin model can improve the diagnosis and prognosis of crack growth using DBN and observation data.

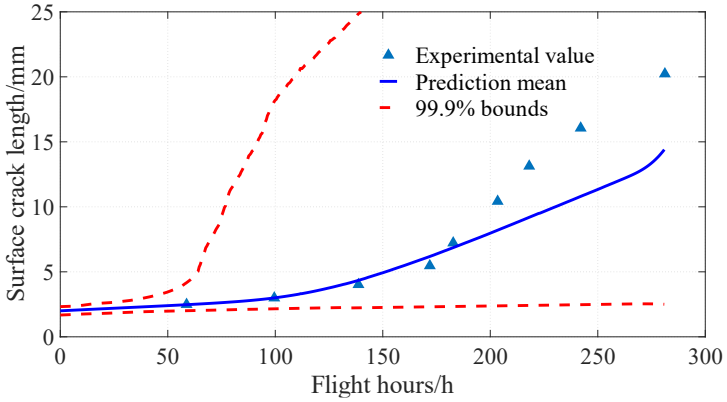

a) Without diagnosis

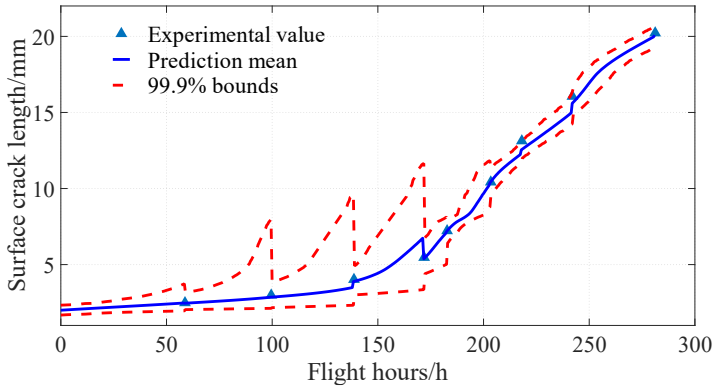

b) With diagnosis

Fig. 9 Comparison of probabilistic crack growth with and without diagnosis.

Table 4 Comparison of diagnosis results of probabilistic crack growth prediction with experimental values

Number of inspections	1	2	3	4	5	6	7	8	9
Time of inspection (h)	58.7	99.5	138.7	171.9	182.7	203.4	218.1	242.0	281.2
Experimental values (mm)	2.49	2.99	4.02	5.47	7.22	10.42	13.13	16.06	20.23
Prediction means (mm)	2.46	2.87	3.88	5.38	7.17	10.36	12.54	15.61	20.08
Relative error (%)	1.20	4.01	3.48	1.65	0.69	0.58	4.49	2.80	0.74
Prediction variance (mm^2)	0.022	0.048	0.096	0.106	0.056	0.073	0.036	0.051	0.029

V. Demonstration of Intelligent Inspection Strategy with a Group of Hypothetical Crack Growth Histories

A. Setting of Relevant Parameters in the Strategy

In this section, a group of hypothetical crack growth histories are simulated to demonstrate the proposed digital-twin-based inspection strategy as an enhancement of the current practice of fixed inspection intervals.

The EIFS distribution for these crack growth histories is set as $\ln a \sim N(-2.65, 0.297^2)$ according to [56]. The initial crack size distribution for the probabilistic damage tolerance is set as a Weibull distribution with mean value of 1.27 mm, standard deviation of 0.116 mm and a Weibull offset of 1.134 mm according to [39]. The critical crack size $a_c = 3.3\,\text{mm}$, calculated by the maximum load in the load spectrum and a safety factor of 1.5 according to FAR-25.303. Instead of the deterministic value, the fracture toughness K_c is assumed to follow $f_{K_c} = N(33.4, 3.34^2)$.

The critical PoF used to calculate inspection intervals is set as 10^{-7} according to [57]. If the traditional particle filtering method is used to estimate the PoF, at least 10^9 particles are required. Some researchers have suggested

several methods to calculate PoF in a lower computational cost [58, 59]. This paper adopts the kernel density estimation (KDE) [60] to fit the PDF of the maximum SIF with a certain number of samples, which may lead to oscillations in the PoF curve but is easy to implement. The fitted PDF is recorded as f_K. Then, the stress-intensity interference theory [61] is used to calculate the PoF:

$$\mathrm{PoF}=\int_{-\infty}^{\infty} f_K(K)\left[\int_{-\infty}^{K} f_{K_c}(K_c)dK_c\right]dK \tag{11}$$

Different sample numbers are used to calculate the first inspection time, and the statistical results are shown in Table 5, which shows that 100,000 samples are sufficient to calculate the inspection time accurately.

Table 5 Calculation of the first inspection time with different number of samples

Sample number	Mean value (h)	Standard deviation (h)
10,000	71.6	8.4
50,000	67.8	2.5
100,000	60.8	1.2
150,000	60.5	0.6
200,000	61.1	0.6

The number of detections N_{det} per inspection is set as 10 when $\bar{\boldsymbol{a}}^{surf}$ is smaller than a_d=1.27mm to balance simulation accuracy and inspection cost. It is worth noting that the $N_{det}=10$ here is used to demonstrate the strategy, which should be determined by the engineering requirements in practical. Other parameters for the diagnosis and prognosis of the probabilistic crack growth are the same as those in Section IV. For the sake of explanation, this paper stipulates that when a_{obs} exceeds $a_e=2$ mm, the lifting frame should be replaced; when it does not exceed 2 mm, the digital twin model should be updated to continue calculating the next inspection time and predicting probabilistic crack growth.

B. Demonstration of the Intelligent Inspection Strategy

Three crack growth histories with different crack growth model parameters and initial crack sizes as shown in Table 6 are assumed, and the proposed inspection strategy is applied to each of them. The results are shown in Fig. 10.

Table 6 Setting of relevant parameters of the three crack growth histories

Serial number	1	2	3
a_0 (mm)	0.0882	0.0816	0.1139
$logC$	-10.7879	-11.1947	-10.7172
γ	2.9108	3.0702	2.9067
K_c $(MPa\sqrt{m})$	34.4647	29.0323	31.9518

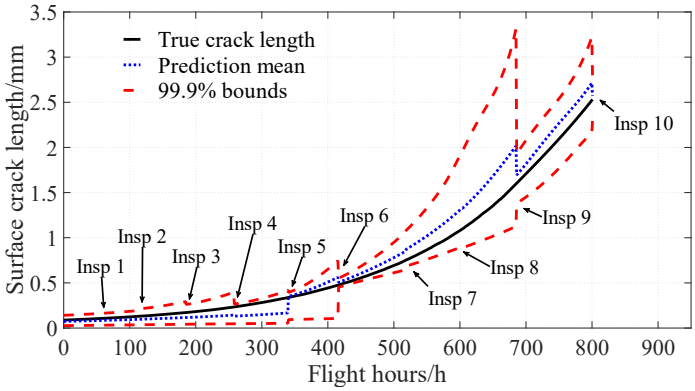

a) The inspections of the first crack growth history.

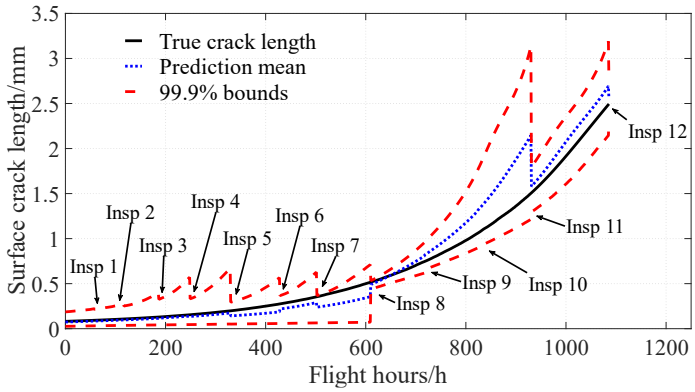

b) The inspections of the second crack growth history.

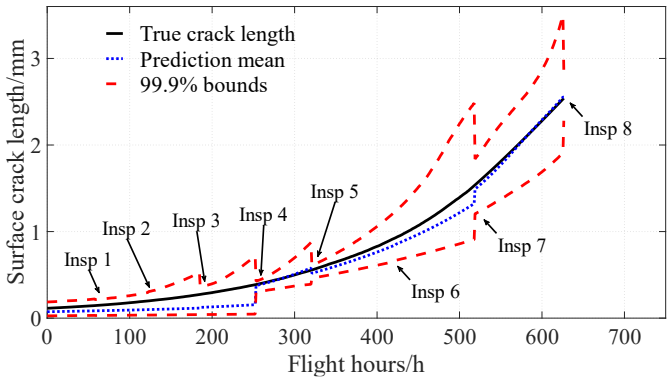

c) The inspections of the third crack growth history.

Fig. 10 The inspections of the three crack growth histories (Insp: abbreviation for inspection).

It can be seen from these results that, compared with traditional fixed inspection intervals based on damage tolerance, the proposed method formulates adaptive inspection intervals based on the updating of the digital twin model. It is worth mentioning that the first inspection time of these three crack growth histories is basically the same, due to that the same process noise is assumed, and the same prior distribution is used for the crack growth model parameters and initial crack size. However, since the difference of these three true crack growth histories, the model parameters *logC* and γ were updated to varying degrees at each inspection, resulting in the difference for the subsequent inspections. The updates of model parameters for the three crack growth histories are listed in Fig. 11 (only the most updated ones are drawn for clarity), from which we can see that the joint distributions gradually become narrower and approach the true values with the updating of the digital twin model, resulting in prediction results closer to the true crack length. The evolution of the PoF used to calculate the inspection intervals is shown in Fig. 12. Once the PoF exceeds 10^{-7}, due to the update of the model, its value will decline rapidly and then gradually rise until the next critical condition arrives.

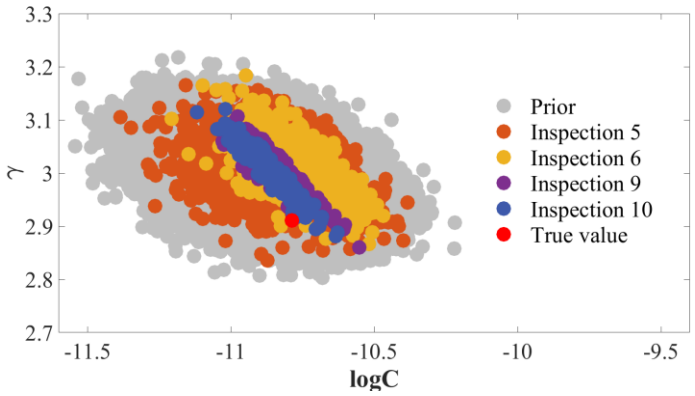

a) The updating of the first crack growth history.

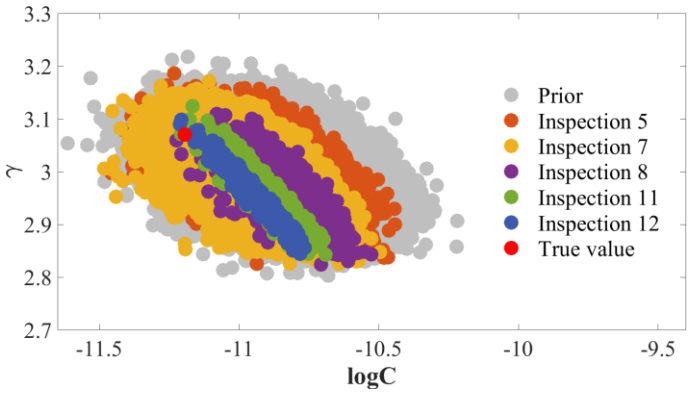

b) The updating of the second crack growth history.

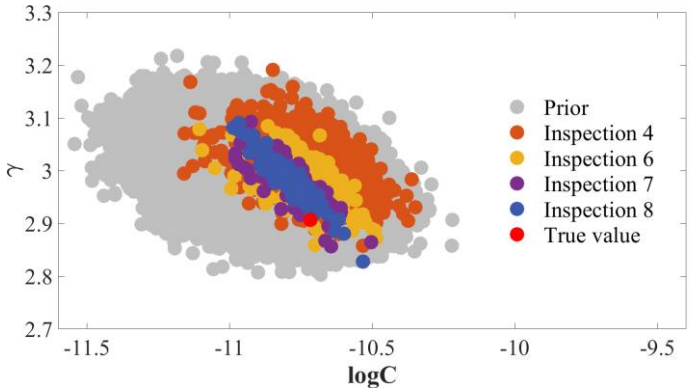

c) The updating of the third crack growth history.

Fig. 11 Updating of joint distribution of logC and γ of the three crack growth histories.

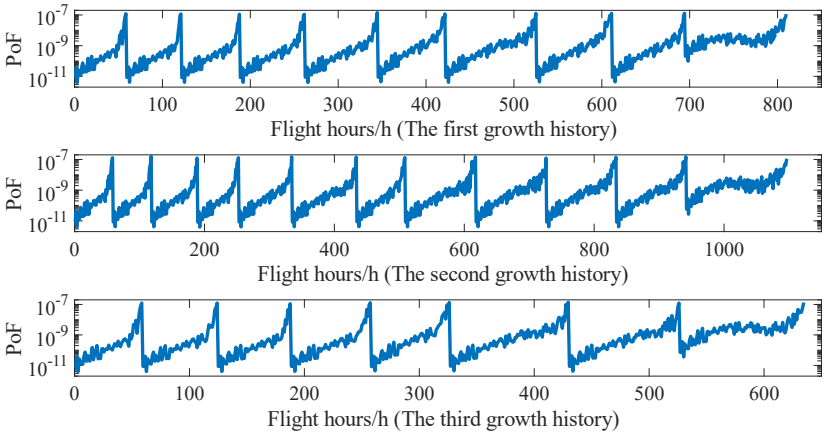

Fig. 12 Calculation of PoF of the three crack growth histories in the second process.

C. Comparison of PoF corresponding to several inspection interval setting methods

In order to illustrate the rationality of the proposed method, the PoF during the service (calculated from the EIFS distribution of the initial crack size), derived from the proposed strategy is compared with that from traditional fixed inspection intervals. According to the obtained critical crack size a_c, the fixed inspection interval is obtained by dividing the crack growth time from $a_d = 1.27$ mm to $a_c = 3.3$ mm by a factor of 2 [62], and the calculation result is 126 h. The calculation method for PoF during the service based on a fixed inspection interval is divided into two cases according to whether updating is carried out during inspection:

(1) Without update: The PoF is calculated from the EIFS distribution, and the model is not updated at each inspection.

(2) With update: At each inspection, the model is updated using the method mentioned in Section II, and then the updated model is used to continue calculating the PoF.

The calculated PoF evolution corresponding to the three hypothetical histories using different inspection interval formulation methods is shown in Fig. 13. In addition, the true PoF calculated by the true crack growth model parameters and initial crack size in Table 6 and only considering the load uncertainty is also shown. Although it is called the "true" PoF here, it is a reference for simulation results to a certain degree. The true PoF is difficult to obtain in a practical environment, and our knowledge of the PoF is still very subjective, in line with the Bayesians. It is to be noted that the calculated PoF curves have some oscillations due that the number of particles is not very large. The PoF corresponding to the fixed inspection interval without update will exceed the critical value of 10^{-7} relatively quickly. In the case of fixed inspection intervals with updates, the PoF is effectively controlled due to model updates in several inspections. However, due to the unreasonable arrangement of inspection intervals, the PoF of the three crack growth histories significantly exceeded the critical value during the service life. For the adaptive inspection strategy proposed in this paper, because the critical PoF is considered when calculating the inspection interval, the value of PoF will be less than the critical value for most of the time until the final inspection.

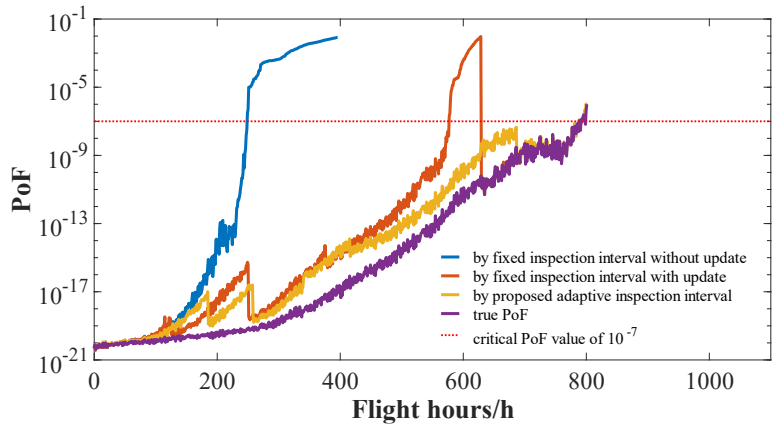

a) The PoF for the first crack growth history.

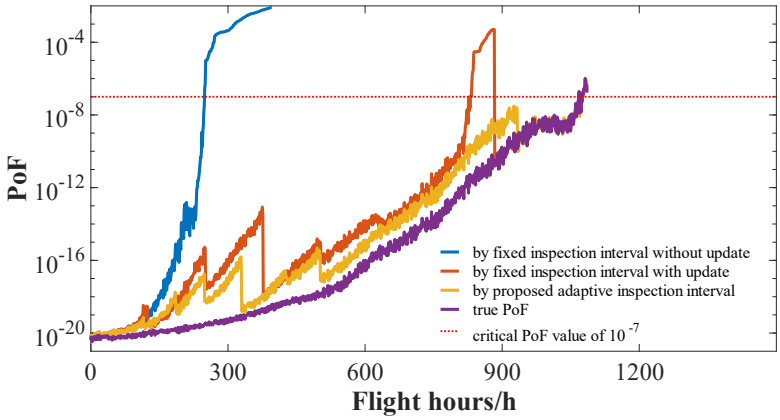

b) The PoF for the second crack growth history.

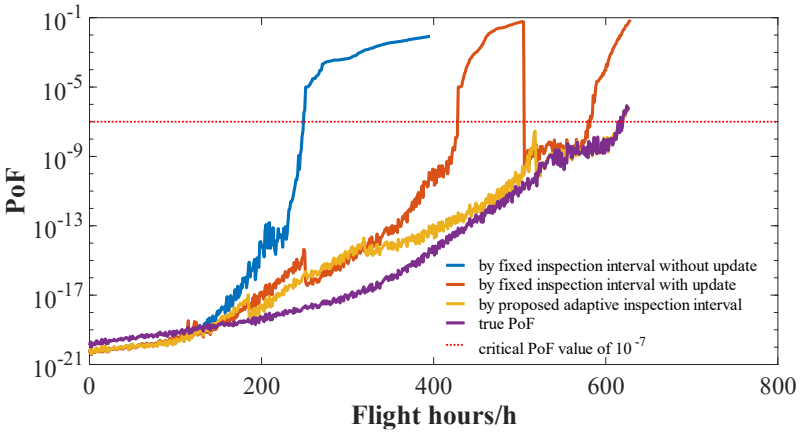

c) The PoF for the third crack growth history.

Fig. 13 Calculation of PoF during service of the three crack growth histories.

In addition, instead of calculating the inspection intervals from a relatively large crack size distribution (the Weibull distribution with a mean value of 1.27 mm) as proposed in Section II, based on critical PoF, some methods [13] calculate the inspection intervals from the EIFS distribution, which may cause safety risks in some special cases.

The fourth crack growth history is used to illustrate this situation, and its initial crack size, *logC* and γ are set as 0.16 mm, -10.45 and 3.0452, respectively, which beyond the values in the prior distribution, indicating an incorrect prior. According to the analysis, the PoF reaches the critical value at 249 h, when the crack size corresponding to this history is 3.4 mm that exceeds a_c and a safety risk exists before the scheduled inspection. The results of inspections, parameter updating, PoF for calculating inspection intervals and the PoF during service obtained by the proposed method are shown in Fig. 14, which indicate that the proposed method can carry out effective inspections on the premise of ensuring security.

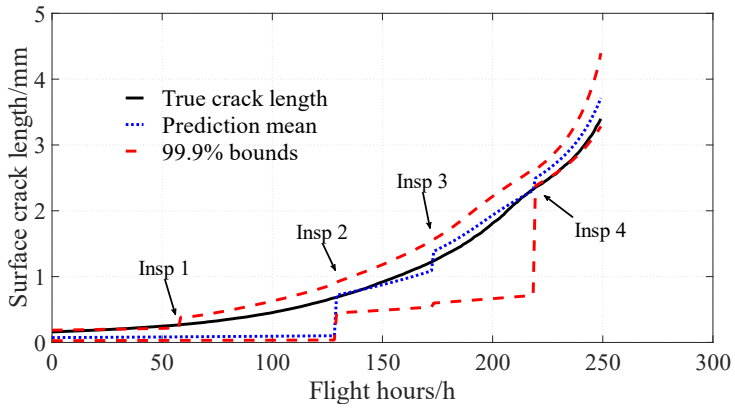

a) The inspections.

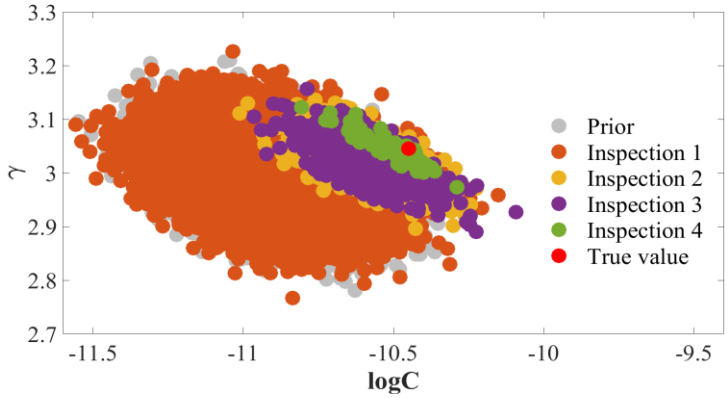

b) The parameter updating.

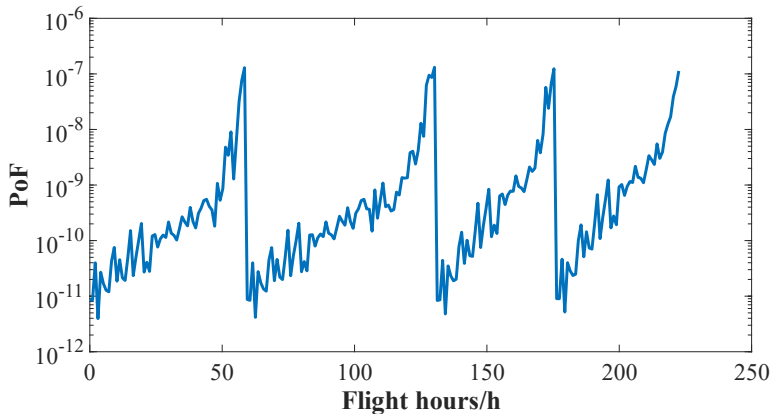

c) PoF for calculating inspection intervals.

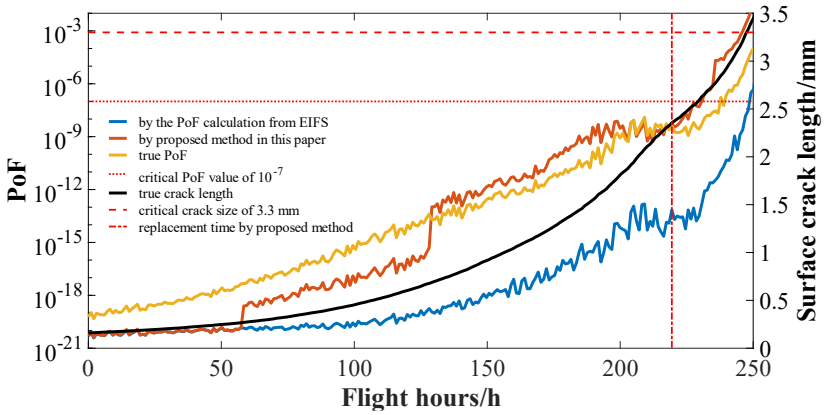

d) Comparation with the method of PoF calculation from EIFS.

Fig. 14 The analysis results of the fourth crack growth history.

In addition, the number of inspections corresponding to several different inspection strategies are compared, as shown in Table 7. The number of inspections corresponding to the strategy proposed in this paper is larger than that corresponding to other methods. However, as we mentioned above, PoF is a kind of subjective awareness to a certain degree and can be controlled effectively by our proposed strategy, which would be helpful for the decision-making process of aircraft inspection and maintenance. Flexible improvements to the strategy may also be made in subsequent efforts to reduce the number of inspections while still maintaining security.

Table 7 Comparison of number of inspections corresponding to different methods

The number of crack growth history	1	2	3	4
Fixed inspection intervals (with and without update)	6	8	5	2
Inspection intervals calculated from EIFS	1	1	1	1
Proposed adaptive inspection intervals	10	12	8	4

VI. Conclusion

In this paper, a crack inspection strategy based on the digital twin is proposed. In this strategy, two probabilistic processes, the primary process for the diagnosis and prognosis of each component and the secondary process for the determination of inspection intervals, are conducted simultaneously, which share the distributions of damage related parameters. The primary process adopts the EIFS as the initial crack distribution to predict the crack growth in real time. Meanwhile, the secondary process adopts the initial distribution as in probabilistic DTA or updated crack distribution and calculates the inspection intervals based on critical PoF. Compared with the traditional inspection strategy, the inspection interval can be dynamically adjusted according to the updating of the digital twin model, and conversely the crack distribution and model parameters are updated based on inspection results, which creates virtuous circles, allowing inspection intervals to be scheduled to better match the safety and economic needs of each aircraft. It is worth mentioning that the proposed inspection strategy is still based on the philosophy of damage tolerance, so it can be seamlessly applied to the inspection of existing aircraft structures.

A round-robin helicopter component is used to demonstrate the present strategy. The digital twin model based on the DBN and ROM is first validated using available experimental data, and the results show that the digital twin model can update itself using measured data to improve the accuracy of damage prognosis. Based on this, the proposed inspection strategy is then applied to several hypothetical crack growth histories, each with different initial crack sizes as well as damage model parameters. The results demonstrated that, while ensuring safety, the inspection intervals can be adaptively arranged with the continuous update of the digital twin model.

In future research, we will further consider more complex forms of structural damage, such as three-dimensional non-planar cracks, composite delamination, etc., and carry out validation of the proposed strategy on more realistic structures.

Acknowledgments

The National Natural Science Foundation of China (grant number 12072011), the Aeronautical Science Foundation of China (grant number 201909051001) supported the work of the first four authors. The China Scholarship Council (grant number 202106020002) and the Academic Excellence Foundation of BUAA for PhD Students supported the work of the second author. The authors express gratitude to Prof. Rhys Jones at Monash University for providing the Asterix spectrum.

References

[1] Myötyri, E., Pulkkinen, U., and Simola, K., "Application of Stochastic Filtering for Lifetime Prediction," Reliability Engineering & System Safety, Vol. 91, No. 2, 2006, pp. 200-208. https://doi.org/10.1016/j.ress.2005.01.002

[2] Sun, J., Zuo, H., Wang, W., and Pecht, M. G., "Prognostics Uncertainty Reduction by Fusing on-Line Monitoring Data Based on a State-Space-Based Degradation Model," Mechanical Systems and Signal Processing, Vol. 45, No. 2, 2014, pp. 396-407. https://doi.org/10.1016/j.ymssp.2013.08.022

[3] Shahani, A., and Mohammadi, S., "Damage Tolerance Approach for Analyzing a Helicopter Main Rotor Blade," Engineering Failure Analysis, Vol. 57, Jul. 2015, pp. 56-71. https://doi.org/10.1016/j.engfailanal.2015.07.025

[4] Li, C., Mahadevan, S., Ling, Y., Choze, S., and Wang, L., "Dynamic Bayesian Network for Aircraft Wing Health Monitoring Digital Twin," AIAA Journal, Vol. 55, No. 3, 2017, pp. 930-941. https://doi.org/10.2514/1.J055201

[5] Wang, Y., Binaud, N., Gogu, C., Bes, C., and Fu, J., "Determination of Paris' Law Constants and Crack Length Evolution via Extended and Unscented Kalman Filter: An Application to Aircraft Fuselage Panels," Mechanical Systems and Signal Processing, Vol. 80, May 2016, pp. 262-281. https://doi.org/10.1016/j.ymssp.2016.04.027

[6] Wallace, M., Azzam, H., and Newman, S., "Indirect Approaches to Individual Aircraft Structural Monitoring," Proceedings of the Institution of Mechanical Engineers, Part G: Journal of Aerospace Engineering, Vol. 218, No. 5, 2004, pp. 329-346. https://doi.org/10.1243/0954410042467059

[7] Levinski, O., Carrese, R., Conser, D., Marzocca, P., and McDonald, M., "OPERAND: An Innovative Multi-Physics Approach to Individual Aircraft Tracking," 18th Australian International Aerospace Congress, Engineers Australia, Royal Aeronautical Soc., Melbourne, Australia, 2019, pp. 1-6.

[8] De Jonge, J., "Monitoring Load Experience of Individual Aircraft," Journal of Aircraft, Vol. 30, No. 5, 1993, pp. 751-755. https://doi.org/10.2514/3.46407

[9] Lee, H., Cho, H., and Park, S., "Review of the F-16 Individual Aircraft Tracking Program," Journal of Aircraft, Vol. 49, No. 5, 2012, pp. 1398-1405. https://doi.org/10.2514/1.C031692

[10] Glaessgen, E., and Stargel, D., "The Digital Twin Paradigm for Future NASA and U.S. Air Force Vehicles," 53rd AIAA/ASME/ASCE/AHS/ASC structures, structural dynamics and materials conference, Honolulu, Hawaii, 2012, p. 1818.

[11] Grieves, M., "Digital Twin: Manufacturing Excellence Through Virtual Factory Replication," White Paper, Vol. 1, Oct. 2014,

pp. 1-7.

[12] Tuegel, E. J., Ingraffea, A. R., Eason, T. G., and Spottswood, S. M., "Reengineering Aircraft Structural Life Prediction Using a Digital Twin," International Journal of Aerospace Engineering, Vol. 2011, Oct. 2011, p. 154798. https://doi.org/10.1155/2011/154798

[13] Millwater, H., Ocampo, J., and Crosby, N., "Probabilistic Methods for Risk Assessment of Airframe Digital Twin Structures," Engineering Fracture Mechanics, Vol. 221, Sept. 2019, p. 106674. https://doi.org/10.1016/j.engfracmech.2019.106674

[14] Cheung, C., and Bellinger, N. C., "Roadmap for Helicopter Life Usage Monitoring," Thirteenth Australian International Aerospace Congress, Royal Aeronautical Soc., Melbourne, Australia, 2009, pp. 1-13.

[15] Zhu, J., Zhang, W., and Li, X., "Fatigue Damage Assessment of Orthotropic Steel Deck Using Dynamic Bayesian Networks," International Journal of Fatigue, Vol. 118, Aug. 2019, pp. 44-53. https://doi.org/10.1016/j.ijfatigue.2018.08.037

[16] Ye, Y., Yang, Q., Yang, F., Huo, Y., and Meng, S., "Digital Twin for the Structural Health Management of Reusable Spacecraft: A Case Study," Engineering Fracture Mechanics, Vol. 234, May 2020, p. 107076. https://doi.org/10.1016/j.engfracmech.2020.107076

[17] Yu, J., Song, Y., Tang, D., and Dai, J., "A Digital Twin Approach Based on Nonparametric Bayesian Network for Complex System Health Monitoring," Journal of Manufacturing Systems, Vol. 58, Aug. 2020, pp. 293-304. https://doi.org/10.1016/j.jmsy.2020.07.005

[18] Karve, P. M., Guo, Y., Kapusuzoglu, B., Mahadevan, S., and Haile, M. A., "Digital Twin Approach for Damage-Tolerant Mission Planning under Uncertainty," Engineering Fracture Mechanics, Vol. 225, Nov. 2020, p. 106766. https://doi.org/10.1016/j.engfracmech.2019.106766

[19] Sisson, W., Karve, P., and Mahadevan, S., "Digital Twin Approach for Component Health-Informed Rotorcraft Flight Parameter Optimization," AIAA Journal, Vol. 60, No. 3, 2022, pp. 1923-1936. https://doi.org/10.2514/1.J060770

[20] Sisson, W., Karve, P., and Mahadevan, S., "Digital Twin for Component Health- and Stress-Aware Rotorcraft Flight Control," Structural and Multidisciplinary Optimization, Vol. 65, No. 11, 2022, pp. 1-12. https://doi.org/10.1007/s00158-022-03413-8

[21] Zhou, X., He, S., Dong, L., and Atluri, S. N., "Real-Time Prediction of Probabilistic Crack Growth with a Helicopter Component Digital Twin," AIAA Journal, Vol. 60, No. 4, 2022, pp. 1-13. https://doi.org/10.2514/1.J060890

[22] Morse, L., Khodaei, Z. S., and Aliabadi, M., "A multi-fidelity modelling approach to the statistical inference of the equivalent

initial flaw size distribution for multiple-site damage," International Journal of Fatigue, Vol. 120, Mar. 2019, pp. 329-341. https://doi.org/10.1016/j.ijfatigue.2018.11.010

[23] Zhuang, M., Morse, L., Khodaei, Z. S., and Aliabadi, M., "Statistical inference of the Equivalent Initial Flaw Size Distribution for an anisotropic material with the Dual Boundary Element Method," International Journal of Fatigue, Vol. 158, May. 2022, p. 106702. https://doi.org/10.1016/j.ijfatigue.2021.106702

[24] Morse, L., Sharif Khodaei, Z., and Aliabadi, M. H., "Statistical Inference of the Equivalent Initial Flaw Size for Assembled Plate Structures with the Dual Boundary Element Method," Engineering Fracture Mechanics, Vol. 238, Oct. 2020, p. 107271. https://doi.org/10.1016/j.engfracmech.2020.107271

[25] Liao, M., Renaud, G., and Bombardier, Y., "Airframe Digital Twin Technology Adaptability Assessment and Technology Demonstration," Engineering Fracture Mechanics, Vol. 225, Nov. 2019, p. 106793. https://doi.org/10.1016/j.engfracmech.2019.106793

[26] Lazzeri, L., and Mariani, U., "Application of Damage Tolerance Principles to the Design of Helicopters," International Journal of Fatigue, Vol. 31, No. 6, 2009, pp. 1039-1045. https://doi.org/10.1016/j.ijfatigue.2008.05.010

[27] Tiong, U. H., and Jones, R., "Damage Tolerance Analysis of a Helicopter Component," International Journal of Fatigue, Vol. 31, No. 6, 2009, pp. 1046-1053. https://doi.org/10.1016/j.ijfatigue.2008.05.012

[28] Dong, L., and Atluri, S. N., "SGBEM(Using Non-Hyper-Singular Traction BIE), and Super Elements, for Non-Collinear Fatigue-Growth Analyses of Cracks in Stiffened Panels with Composite-Patch Repairs," Computer Modeling in Engineering & Sciences(CMES), Vol. 89, No. 5, 2012, pp. 415-456. https://doi.org/10.3970/cmes.2012.089.417

[29] Dong, L., and Atluri, S. N., "Fracture & Fatigue Analyses: SGBEM-FEM or XFEM? Part 1: 2D Structures," CMES: Computer Modeling in Engineering & Sciences, Vol. 90, No. 2, 2013, pp. 91-146. https://doi.org/10.3970/cmes.2013.090.091

[30] Dong, L., and Atluri, S. N., "Fracture & Fatigue Analyses: SGBEM-FEM or XFEM? Part 2: 3D Solids," CMES: Computer Modeling in Engineering & Sciences, Vol. 90, No. 5, 2013, pp. 379-413. https://doi.org/10.3970/cmes.2013.090.379

[31] Welch, G., Bishop, G., and Hill, C., An Introduction to the Kalman Filter, US Tech Reps Inc., Chapel Hill, NC, 2000, pp. 127-132.

[32] Khorasgani, H., Biswas, G., and Sankararaman, S., "Methodologies for System-Level Remaining Useful Life Prediction,"

Reliability Engineering & System Safety, Vol. 154, May 2016, pp. 8-18.
https://doi.org/10.1016/j.ress.2016.05.006

[33] Julier, S. J., and Uhlmann, J. K., "New Extension of the Kalman Filter to Nonlinear Systems," Signal Processing, Sensor Fusion, and Target Recognition VI, International Society for Optics and Photonics, Orlando, 1997, pp. 182-193.

[34] Fan, J., Yung, K.-C., and Pecht, M., "Prognostics of Chromaticity State for Phosphor-Converted White Light Emitting Diodes Using an Unscented Kalman Filter Approach," IEEE transactions on device, Vol. 14, No. 1, 2013, pp. 564-573.
https://doi.org/10.1109/TDMR.2013.2283508

[35] Al-Hussein, A., and Haldar, A., "Unscented Kalman Filter with Unknown Input and Weighted Global Iteration for Health Assessment of Large Structural Systems," Structural Control and Health Monitoring, Vol. 23, No. 1, 2016, pp. 156-175.
https://doi.org/10.1002/stc.1764

[36] Arulampalam, M. S., Maskell, S., Gordon, N., and Clapp, T., "A Tutorial on Particle Filters for Online Nonlinear/Non-Gaussian Bayesian Tracking," IEEE Transactions on Signal Processing, Vol. 50, No. 2, 2002, pp. 174-188.
https://doi.org/10.1109/78.978374

[37] Sun, J., Zuo, H., Wang, W., and Pecht, M. G., "Application of a State Space Modeling Technique to System Prognostics Based on a Health Index for Condition-Based Maintenance," Mechanical Systems and Signal Processing, Vol. 28, Oct. 2011, pp. 585-596.
https://doi.org/10.1016/j.ymssp.2011.09.029

[38] Hu, Y., Baraldi, P., Di Maio, F., and Zio, E., "A Particle Filtering and Kernel Smoothing-Based Approach for New Design Component Prognostics," Reliability Engineering & System Safety, Vol. 134, Oct. 2014, pp. 19-31.
https://doi.org/10.1016/j.ress.2014.10.003

[39] Millwater, H. R., and Wieland, D. H., "Probabilistic Sensitivity-Based Ranking of Damage Tolerance Analysis Elements," Journal of Aircraft, Vol. 47, No. 1, 2010, pp. 161-171.
https://doi.org/10.2514/1.44498

[40] Grooteman, F., "A Stochastic Approach to Determine Lifetimes and Inspection Schemes for Aircraft Components," International Journal of Fatigue, Vol. 30, No. 1, 2008, pp. 138-149.
https://doi.org/10.1016/j.ijfatigue.2007.02.021

[41] Jones, R., Baker, A., Matthews, N., and Champagne, V., Aircraft Sustainment and Repair, Butterworth-Heinemann, Oxford, 2017, pp. 136-138.

[42] Kim, J., Le, M., Lee, J., and Hwang, Y. H., "Eddy Current Testing and Evaluation of Far-Side Corrosion around Rivet in Jet-Engine Intake of Aging Supersonic Aircraft," Journal of Nondestructive Evaluation, Vol. 33, No. 4, 2014, pp. 471-480.
https://doi.org/10.1007/s10921-014-0242-z

[43] Ling, Y., Asher, I., Wang, L., Viana, F., and Khan, G., "Information Gain-Based Inspection Scheduling for Fatigued Aircraft Components," 19th AIAA Non-Deterministic Approaches Conference, American Institute of Aeronautics and Astronautics, Inc., Grapevine, Texas, 2017, p. 1565.

[44] Cansdale, R., and Perrett, B., "The Helicopter Damage Tolerance Round Robin Challenge," Workshop on Fatigue Damage of Helicopters, Vol. 12, Univ. of Pisa, Pisa, Italy, 2002, pp. 99–128.

[45] Krishnapillai, K., and Jones, R., "Fatigue Based 3D Structural Design Optimisation Implementing Genetic Algorithms and Utilising the Generalised Frost-Dugdale Crack Growth Law," Proceedings of the 9th WSEAS International Conference on Evolutionary Computing, World Scientific and Engineering Academy and Society, Sofia, Bulgaria, 2007, pp. 1-13.

[46] Barter, S., Molent, L., Goldsmith, N., and Jones, R., "An Experimental Evaluation of Fatigue Crack Growth," Engineering Failure Analysis, Vol. 12, No. 1, 2005, pp. 99-128.
https://doi.org/10.1016/j.engfailanal.2004.04.002

[47] Frost, N., and Dugdale, D., "The Propagation of Fatigue Cracks in Sheet Specimens," Journal of the Mechanics Physics of Solids, Vol. 6, No. 2, 1958, pp. 92-110.
https://doi.org/10.1016/0022-5096(58)90018-8

[48] Newman Jr, J., Irving, P., Lin, J., and Le, D. D., "Crack Growth Predictions in a Complex Helicopter Component under Spectrum Loading," Fatigue & Fracture of Engineering Materials & Structures, Vol. 29, No. 11, 2006, pp. 949-958.
https://doi.org/10.1111/j.1460-2695.2006.01053.x

[49] Hombal, V., and Mahadevan, S., "Surrogate Modeling of 3D Crack Growth," International Journal of Fatigue, Vol. 47, Aug. 2012, pp. 90-99.
https://doi.org/10.1016/j.ijfatigue.2012.07.012

[50] Pidaparti, R., and Palakal, M., "Neural network approach to fatigue-crack-growth predictions under aircraft spectrum loadings," Journal of Aircraft, Vol. 32, No. 4, 1995, pp. 825-831.
https://arc.aiaa.org/doi/10.2514/3.46797

[51] Cherepanov, G. P., and Cooley, W., Mechanics of Brittle Fracture, McGraw-Hill International Book Co., New York, 1979.

[52] Yang, J., and Manning, S., "Stochastic Crack Growth Analysis Methodologies for Metallic Structures," Engineering Fracture Mechanics, Vol. 37, No. 5, 1990, pp. 1105-1124.
https://doi.org/10.1016/0013-7944(90)90032-C

[53] Chen, J., Yuan, S., and Jin, X., "On-Line Prognosis of Fatigue Cracking via a Regularized Particle Filter and Guided Wave Monitoring," Mechanical Systems and Signal Processing, Vol. 131, May. 2019, pp. 1-17.
https://doi.org/10.1016/j.ymssp.2019.05.022

[54] Corbetta, M., Sbarufatti, C., Giglio, M., and Todd, M. D., "Optimization of Nonlinear, Non-Gaussian Bayesian Filtering for

Diagnosis and Prognosis of Monotonic Degradation Processes," Mechanical Systems and Signal Processing, Vol. 104, Nov. 2017, pp. 305-322.
https://doi.org/10.1016/j.ymssp.2017.11.012

[55] Bergner, F., and Zouhar, G., "A new approach to the correlation between the coefficient and the exponent in the power law equation of fatigue crack growth," International Journal of Fatigue, Vol. 22, No. 3, 2000, pp. 229-239.
https://doi.org/10.1016/S0142-1123(99)00123-1

[56] Wu, J. Y., Shiao, M., Shin, Y., and Stroud, W. J., "Reliability-Based Damage Tolerance Methodology for Rotorcraft Structures," Journal of Materials and Manufacturing, Vol. 113, Mar. 2004, pp. 295-305.
https://doi.org/10.4271/2004-01-0681

[57] Lincoln, J. W., "Risk assessment of an aging military aircraft," Journal of aircraft, Vol. 22, No. 8, 1985, pp. 687-691.
https://doi.org/10.2514/3.45187

[58] Wang, L., Asher, I., Atkinson, S., Khan, G., Longtin, R., Ball, D., Shannon, R., Dakwar, E., and Hoffmann, J., "AIRFRAME DIGITAL TWIN (ADT) Delivery Order FA8650-17-F-2219: Scalable, Accurate, Flexible, Efficient, Robust, Prognostic and Probabilistic Individual Aircraft Tracking (SAFER-P2IAT) Full-Scale Demonstration Experiment," GENERAL ELECTRIC CO NISKAYUNA NY NISKAYUNA United States, 2019.

[59] Crosby, N., "Efficient Adaptive Importance Sampling Estimation of Time Dependent Probability of Failure with Inspections for Damage Tolerant Aircraft Structures," The University of Texas at San Antonio, 2021.

[60] Rosenblatt, M., “Remarks on Some Nonparametric Estimates of a Density Function,” Annals of Mathematical Statistics, Vol. 27, No. 3, 1956, pp. 832–837.
https://doi:10.1214/aoms/1177728190

[61] Bhattacharyya, G., and Johnson, R. A., "Estimation of reliability in a multicomponent stress-strength model," Journal of the American Statistical Association, Vol. 69, No. 348, 1974, pp. 966-970.
https://doi.org/10.1016/0026-2714(93)90362-3

[62] Gallagher, J. P., USAF Damage Tolerant Design Handbook: Guidelines for the Analysis and Design of Damage Tolerant Aircraft Structures: Final Report for Period September 1980 to March 1984, Flight Dynamics Laboratory, Air Force Wright Aeronautical Labortories, 1984.